Large eddy simulation investigation of Reynolds number effects on rheological behavior of Ostwald de Waele fluids

Mohamed Abdi, Meryem Ould-Rouiss, Manel Ait Yahia, Amina Ould Mohamed

Large Eddy Simulation Investigation of Reynolds Number Effects on Rheological Behavior of Ostwald de Waele Fluids

Mohamed ABDI [a*], Meryem OULD ROUISS [b], Manel AIT YAHIA [c], Amina OULD MOHAMED [c].

(a) Laboratoire de génie électrique et des plasmas (LGEP) University of Tiaret, Algeria
(b) Laboratoire de Modélisation et Simulation Multi Echelle, MSME, Université Gustave Eiffel, UMR 8208 CNRS, 5 bd Descartes, 77454 Marne-la-Vallée, Paris, France
(c) Department of Mechanical Engineering, University Ibn Khaldoun, Tiaret 14000, Algeria
**E-mail: abdi.mohamed1@live.fr*

ABSTRACT

A fully developed turbulent pipe flow of non-Newtonian fluids was investigated numerically using the large eddy simulation (LES) method. The rheological and hydrodynamic behaviour of the power-law fluids was a primary focus for flow behaviour indexes of 0.75, 1, and 1.4 and at simulation Reynolds numbers of 4000, 8000, and 12000. The calculations utilised a finite difference method with a numerical resolution of 65^3 grid points in the r, θ and z dimensions, respectively. They were second-order accurate in space and time. According to the results, the shear rate profiles throughout the pipe radius for the pseudoplastic and dilatant fluids noticeably decreased and improved with a higher flow index. Additionally, the elevated flow index caused a notable rise in the fluid viscosity close to the wall, which raised the friction factor.

KEYWORDS: Large eddy simulation (LES); Shear-thinning; Shear-thickening; Fully developed, Turbulent flow.

1. INTRODUCTION

The industry has become very interested in the flow of non-Newtonian fluids since these fluids are used in many technical applications, including the production of cement, food, paper, and paint goods, as well as in the petroleum, pharmaceutical, and polymer processing sectors. A literature review shows that the turbulent flow of non-Newtonian fluids has received significant attention in recent years. Numerous studies have been conducted on the flow of non-Newtonian fluids in axially stationary pipes, using theoretical, experimental, and numerical methods to describe the rheological behaviour and to evaluate the effects of the rheological properties of this type of fluid [1-16]. Pinho et al. [5] used water and four concentrations of a polymer shear-thinning solution (sodium carboxymethyl cellulose) to assess the mean axial velocity and the three normal stresses in fully developed pipe flow in the range of Reynolds numbers from 240 to 111,000. Malin [6] employed a modified version of the Lam-Bremhorst K-ε model in a turbulent flow to simulate numerically fully developed laminar and turbulent flow of power-law fluids at different Reynolds numbers for various power-law indices. Using the spectral element-Fourier approach, Rudman et al. [9] performed a direct numerical simulation (DNS) of shear-thinning fluids at flow behaviour indices of (0.5, 0.69, and 0.75)

More recently, Abdi et al. [17] used LES and an extended Smagorinsky model to perform fully developed turbulent forced convection of thermally independent pseudoplastic fluid via an axially heated rotating conduit. The simulation Reynolds and Prandtl values for the working fluid were set to 4000 and 1, respectively, with a rotation rate ranging from 0 to 3. The temperature along the pipe wall radius is shown to fall as the rotation rate rises pipe wall rotates dramatically due to a centrifugal force that substantially causes the mean axial velocity profile to rise when the apparent fluid viscosity in the pipe core region lowers. The higher-order statistics show that the rotation rate effect on the skewness and flatness coefficients is primarily limited to the region close to the pipe wall. Further away from the pipe wall, these profiles appear to be almost completely independent of the centrifugal force caused by the rotating pipe wall.

Using a large eddy simulation (LES) and a conventional dynamic model, the current work was focused on a fully developed turbulent flow through an isothermal axially stationary pipe of the power-law fluids. This research examined dilatant (shear-thickening) and pseudoplastic (shear-thinning) fluids spanning the range of 0.75 to 1.4 for different Reynolds values (4000, 8000 and 12000). By examining both rheological properties and mean flow quantities, such as the apparent fluid viscosity, the shear stress, the shear rate, the mean axial velocity, and the friction factor, this study investigated the impact of the Reynolds number on the rheological behaviour numerically and on the flow patterns of this type of non-Newtonian fluid.

2. GOVERNING EQUATIONS AND NUMERICAL PROCEDURE

2.1. Governing Equations

The present study was devoted to a fully developed turbulent flow of pseudoplastic (n=0.75), dilatant (n=1.4) and Newtonian (n=1) fluids through an axially stationary pipe with a computation domain of 20R (Fig.1), by employing large eddy simulation (LES) with a standard dynamic model. Three simulation Reynolds numbers (Re_s) were considered in the present study (4000, 8000 and 12000), which was based on the centerline axial velocity of the analytical fully developed laminar profile (U_{CL}), which are defined respectively as $Re_s=\rho U_{CL}^{2-n}R^n/K$ and $U_{CL}=(3n+1).U_b/(n+1)$. U_b is the mean velocity, K is the fluid consistency index, and Re_{MR} is the Reynolds number of Metzner and Reed and is defined as $\mathrm{Re}_{MR}=8\rho D^n U_b^{2-n}\big/K\left(6+2/n\right)^n$.

The filtered equations can be expressed as follows (Equations 1 and 2):

$$\frac{\partial \bar{u}_i}{\partial x_i}=0 \tag{1}$$

$$\frac{\partial \bar{u}_j}{\partial t}+\frac{\partial \bar{u}_i\bar{u}_j}{\partial x_i}=-\frac{d\bar{P}}{\partial x_j}+\frac{1}{\mathrm{Re}_s}\frac{\partial}{\partial x_i}\left[\overline{\dot{\gamma}^{n-1}}\left(\frac{\partial \bar{u}_j}{\partial x_i}+\frac{\partial \bar{u}_i}{\partial x_j}\right)\right]+\frac{\partial \bar{\tau}_{ij}}{\partial x_i} \tag{2}$$

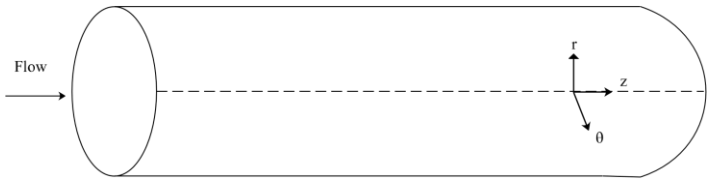

Figure 1: computational domain

2.2. Numerical Procedure

The governing equations were discretised on a staggered mesh in cylindrical coordinates with a computational length in the axial direction 20R. The numerical integration was performed using a finite difference scheme, second-order accurate in space and time. The time advancement employed a fractional-step method. A third-order Runge-Kutta explicit scheme and a Crank-Nicholson implicit scheme were used to evaluate convective and diffusive terms. The above mathematical model was implemented in a finite difference laboratory code. The grid 65^3 grid points in axial, radial and circumferential directions, respectively, were found to provide an accurate prediction of the turbulence statistics, in agreement with the available data of the literature, and give a good compromise between the required CPU-time and accuracy.

3. RESULTS AND DISCUSSION

The rheological properties and mean flow quantities were examined, including the shear rate, apparent viscosity, and mean axial velocity. The friction factor was to explore the influence of the Reynolds number on the rheological and flow patterns of shear-thinning (n<1) and shear thickening (n>1) fluids. The study used LES with a standard dynamic model at three flow behaviour indices (0.75, 1 and 1.4) and three simulation Reynolds numbers (4000, 8000 and 12000).

Figure 2 compares the predicted profile of the turbulent axial velocity of a shear-thinning fluid with a flow index (n) of 0.75 at Reynolds Metzner and Reed number of 4255 with that of DNS data performed by Rudman et al. [9] at Reynolds Metzner and Reed number of 3935. No significant differences were observed between them, where the predicted profile was in good agreement with that of Rudman et al. [9] over the entire flow region.

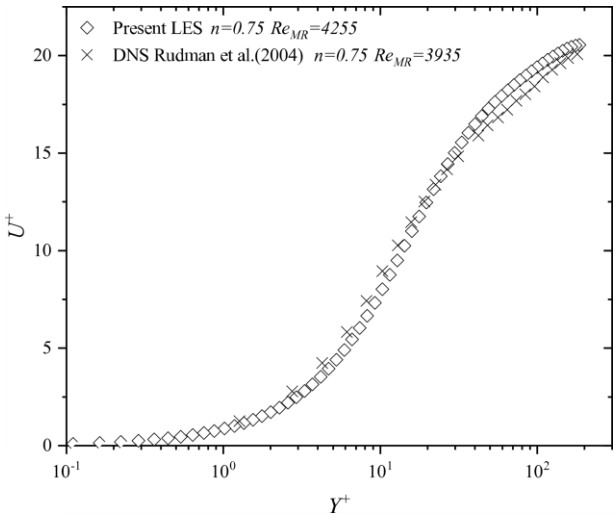

Figure 2: Validation of the results.

3.1. Mean Normalized Shear Rate and Viscosity

The shear rate and apparent viscosity distributions of the shear-thinning and shear-thickening fluids along the pipe radius are depicted in Fig.3 and Fig.4, respectively, against the distance from the wall in wall units Y^+. The flow behaviour indexes were set at 0.75, 1 and 1.4 at a simulation Reynolds number of 4000, 8000 and 12000. As shown in Fig.3 in the viscous sublayer ($0 \leq Y^+ \leq 5$), the shear rate profiles were nearly linear, they remained constant along the near-wall region for the three Reynolds numbers. Beyond ($Y^+=5$), the shear rate profiles began to decrease gradually with distance from the wall (Y^+) towards the core region, where this reduction was sharp in the buffer region ($5 \leq Y^+ \leq 30$) for all cases.

It was evident that the shear rate profile of the pseudoplastic (n=0.75) lay above those of the Newtonian and dilatant (n=1.4) fluids for all Reynolds numbers, where the decreased flow behaviour index resulted in an enhancement in the shear rate along the radial coordinate. On the other hand, the Reynolds number largely affected the shear rate distributions of the power-law fluids along the pipe radius, especially in the near-wall region, where the shear rate profiles of the Reynolds number of 12000 lie above those of 8000 and 4000. With increasing Reynolds number, the shear rate enhanced significantly along the pipe radius, especially in the viscous sublayer. It was worth noting that this trend was more pronounced as the flow behaviour index decreased. The shear rate of the shear-thinning (n=0.75) fluid was more affected by the Reynolds number than those of the Newtonian and shear-thickening (n=1.4) fluids.

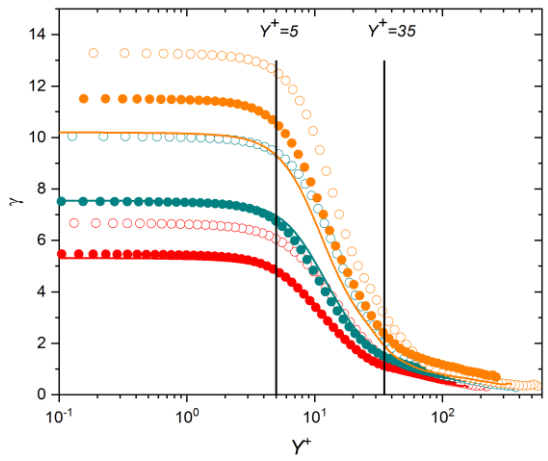

Figure 3: Shear rate profile versus Y^+.

Open symbols: n=0.75; Solid line: n=1 and Closed symbols: n=1.4

Red: Re_s=4000; Blue: Re_s=8000 and Orange: Re_s=12000

As seen in Fig.4, the apparent viscosity of the shear-thinning (n=0.75) and shear-thickening (n=1.4) fluids were identical and equal to the apparent viscosity at the wall (η_w) in the near-wall region for all Reynolds numbers, where no significant noteworthy differences are observed between the three Reynolds numbers. It can be said that the apparent viscosity of the power-law fluids seemed independent of the flow behaviour index and the Reynolds number along the viscous sublayer. Beyond the buffer region (Y^+>5), the apparent viscosity profiles began to deviate from each other significantly further away from the wall, where there was a clear trend of gradually increasing and decreasing in apparent viscosity of the pseudoplastic (n=0.75) and dilatant (n=1.4), respectively with the wall distance (Y^+) towards the core region. The decreased flow behaviour index (n) resulted in a considerable enhancement in the apparent viscosity far away from the wall.

It was apparent in Fig.4 that the viscosity profiles of the Reynolds numbers 4000, 8000 and 12000 collapsed with each other over the entire flow region, where there was no effect of the Reynolds number on the apparent viscosity distribution of the three flow behaviour indices observed. It can be said that the apparent viscosity of the power-law fluids was nearly independent of the Reynolds number along the radial direction.

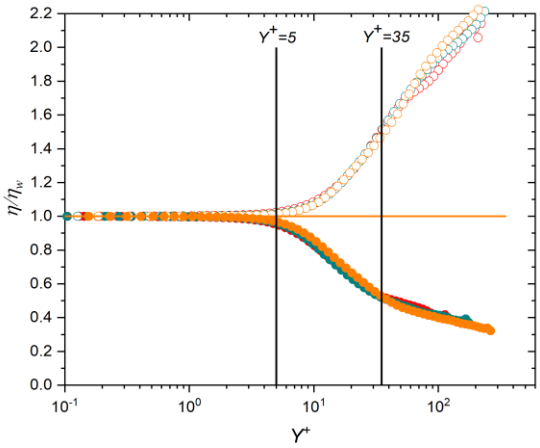

Figure 4: Apparent viscosity profile versus Y^+.

Open symbols: n=0.75; Solid line: n=1 and Closed symbols: n=1.4 *Red: Re_s=4000; Blue: Re_s=8000 and Orange: Re_s=12000.*

Figure 5 illustrates the apparent viscosity profile scaled by the viscosity at the wall (η_w) of the shear-thinning and shear-thickening fluids against the shear rate scaled by the shear rate at the wall ($\dot{\gamma}_w$). As seen in Fig.5 the apparent viscosity of dilatant (n=1.4) increased progressively with the shear rate for all Reynolds numbers, as the Reynolds number decreased as the apparent viscosity enhanced rapidly. On the other hand, the apparent viscosity of the pseudoplastic (n=0.75) fluid was inversely proportional to the shear rate: the shear rate increased as the apparent viscosity decreased considerably for the three Reynolds numbers. It should be noted that the apparent viscosity of the shear-thinning fluid attenuated or diminished rapidly as the Reynolds number decreased.

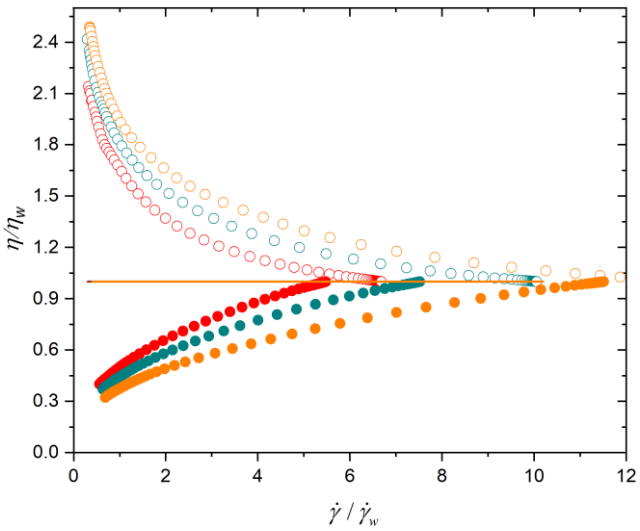

Figure 5: Apparent viscosity against the shear rate.

Open symbols: n=0.75; Solid line: n=1 and Closed symbols: n=1.4 *Red: Re_s=4000; Blue: Re_s=8000 and Orange: Re_s=12000.*

3.2. Turbulent axial Velocity Profile

The turbulent axial velocity profile of the pseudoplastic (n=0.75), dilatant (n=1.4) and Newtonian fluids along the pipe radius scaled by the friction velocity against the distance from the wall in wall units Y^+ is presented in Fig.6, at simulation Reynolds numbers of 4000, 8000 and 12000. The dash lines represented the universal velocity distributions in the viscous sublayer ($0 \leq Y^+ \leq 5$) and in the logarithmic layer ($30 \leq Y^+ \leq 200$). Results showed that in the viscous sublayer, the predicted turbulent axial velocity profile of the three flow behaviour indices (n) was almost identical and agreed with the universal linear law $U^+=Y^+$ up to approximately (Y^+=5) for all Reynolds numbers. It can be said that the turbulent velocity was almost independent of the flow behaviour index and the Reynolds number in the near-wall region. Beyond the buffer region (Y^+>5), the turbulent axial velocity profiles began to deviate significantly from each other with distance from the wall (Y^+), where this deviation became more distinct the further away from the near-wall region. In the logarithmic layer ($30 \leq Y^+ \leq 200$), the profiles of the shear-thinning (n=0.75) fluids lay above those of Newtonian and shear-thickening (n=1.4) fluids for all Reynolds numbers, where this trend was more pronounced as the Reynolds number increased.

It can be said that the turbulent axial velocity was affected largely by the flow index and the Reynolds number out of the buffer region (Y^+>30), where the decreased flow behaviour index led to an enhancement of the apparent viscosity, consequently in the turbulent axial velocity in the logarithmic region for the three Reynolds numbers. Moreover, as the Reynolds number increased, the turbulent velocity enhanced considerably in the logarithmic region, where this improvement was due to the increase in the inertia force.

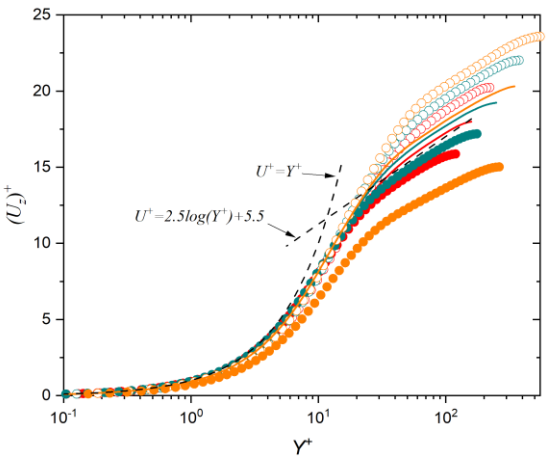

Figure 6: Axial velocity profile versus Y^+.

Open symbols: n=0.75; Solid line: n=1 and Closed symbols: n=1.4 *Red: Re_s=4000; Blue: Re_s=8000 and Orange: Re_s=12000.*

3.3. Friction factor

The friction factor of the pseudoplastic (n=0.75), dilatant (n=1.4) and Newtonian fluids at simulation Reynolds numbers of 4000, 8000 and 12000 are shown in Table 1. The friction factor enhanced gradually with the increase in the flow behaviour index. There was a clear trend of a decrease in the friction factor with an increasing Reynolds number. It was worth noting that the increased Reynolds number induced a marked reduction in the friction factor for the three flow behaviour indices, where this was ascribed to the attenuation in the viscous force near the wall region.

Table 1: Friction factor

Re_s	4000			8000			12000		
n	0.75	1	1.4	0.75	1	1.4	0.75	1	1.4
f.E-1	0.0845	0.107	0.125	0.065	0.0837	0.0977	0.0539	0.0716	0.0833

4. CONCLUSIONS

The numerical analysis of a fully developed turbulent flow of pseudoplastic and dilatant fluids in an axial pipe using LES with a conventional dynamic model was presented. This was carried out for three distinct flow behaviour indices (n=0.75, 1 and 1.4) at three simulated Reynolds number levels (Re_s=4000, 8000, and 12000). This research examined how the Reynolds number affected hydrodynamic and fluid rheological characteristics to characterise this fluid's rheological behaviour and flow patterns in such a situation. The results showed that the Reynolds number rose, and the shear rate of the shear-thinning and thickening fluids was mainly influenced by the Reynolds number over the whole flow zone, which led to an improvement in the shear rate profile along the radial coordinate. When Re had no apparent influence on the viscosity of the three flow behaviour indices, it was concluded that the apparent viscosity of the power-law fluids was almost independent of Re. The turbulent axial velocity in the logarithmic region for the three Reynolds numbers increased in apparent viscosity due to the lowered flow behaviour index. This tendency became more obvious as the Reynolds number rose. Lastly, an increasing Reynolds number significantly attenuated the friction factor for the three flow behaviour indices.

NOMENCLATURE

U_b	Average velocity, $\left(m.s^{-1}\right)$
U_τ	Friction velocity $U_\tau = \left(\tau_w/\rho\right)^{1/2}$, $\left(m.s^{-1}\right)$
U_{CL}	Centreline axial velocity for analytical fully developed laminar profile $U_{CL} = \left(3n+1\right)U_b/\left(n+1\right)$, $\left(m.s^{-1}\right)$
R	Pipe radius, $\left(m\right)$
n	Flow index
K	Consistency index $\left(pa.s^n\right)$
Y^+	Wall distance $Y^+ = \rho U_\tau Y/\eta_w$
f	Friction factor $f = 2\tau_W/\left(\rho U_b{}^2\right)$
Re_s	Reynolds number of the simulations $\mathrm{Re}_s = \rho U_{CL}{}^{2-n} R^n/K$

Greek symbols	
$\dot{\gamma}$	Shear rate $\dot{\gamma} = \sqrt{S_{ij}S_{ij}}$
η	apparent viscosity $\eta = K\dot{\gamma}^{n-1}$
ρ	Density
$\bar{\tau}_{ij}$	Subgrid stress tensor $\bar{\tau}_{ij} = -2\nu_t \bar{S}_{ij}$
Subscripts	
z, r, θ	Axial, radial, tangential velocity
C	Centreline
L	Laminar
s	Simulation
w	Wall
Superscripts	
$\langle\ \rangle$	Statistically averaged
$(\ )^+$	Normalised by U_τ

Figures	Captions
Figure 1	computational domain
Figure 2	Validation of the present results.
Figure 3	Shear rate profile versus Y^+. Open symbols: n=0.75; Solid line: n=1 and Closed symbols: n=1.4 *Red: Re_s=4000; Blue: Re_s=8000 and Orange: Re_s=12000.*
Figure 4	Apparent viscosity profile versus Y^+. Open symbols: n=0.75; Solid line: n=1 and Closed symbols: n=1.4 *Red: Re_s=4000; Blue: Re_s=8000 and Orange: Re_s=12000.*
Figure 5	Apparent viscosity against the shear rate. Open symbols: n=0.75; Solid line: n=1 and Closed symbols: n=1.4 *Red: Re_s=4000; Blue: Re_s=8000 and Orange: Re_s=12000.*
Figure 6	Axial velocity profile versus Y^+. Open symbols: n=0.75; Solid line: n=1 and Closed symbols: n=1.4 *Red: Re_s=4000; Blue: Re_s=8000 and Orange: Re_s=12000.*

Figures list.

Tables	Captions
Table 1	Friction factor

Tables list.

REFERENCES

[1]. A. B. Metzner, and J. C. Reed: Flow of non-Newtonian fluids-correlation of the laminar, transition, and turbulent-flow regions. J. AIChE. vol 1, no. 4 (Dec. 1955) 434-440.

[2]. A. B. Metzner: Non-Newtonian Fluid Flow. Relationships between Recent Pressure-Drop Correlations. Ind. Eng. Chem. vol. 49, no. 9 (Sep 1957) 1429-1432.

[3]. D. W. Dodge and A. B. Metzner: Turbulent flow of non-newtonian systems. AIChE J. vol. 5, no. 2 (Jun. 1959) 189-204.

[4]. V. Vidyanidhi and A. Sithapathi: Non-Newtonian Flow in a Rotating Straight Pipe. J. Phys. Soc. Japan, vol. 29, no. 1. (Jul. 1970) pp. 215–219.

[5]. F. T. Pinho and J. H. Whitelaw: Flow of non-newtonian fluids in a pipe. J. Nonnewton. Fluid Mech., vol. 34, no. 2. (Jan. 1990) pp. 129-144.
[6]. M. R. Malin: Turbulent pipe flow of power-law fluids. Int. Commun. Heat Mass Transf., vol. 24, no. 7. (Nov. 1997) pp. 977-988.
[7]. M. Malin: the Turbulent Flow of Bingham Plastic Fluids in Smooth Circular Tubes. Int. Commun. Heat Mass Transf. vol. 24, no. 6 (Oct 1997) pp. 793-804.
[8]. M. Malin: Turbulent pipe flow of Herschel-Bulkley fluids. Int. Commun. Heat Mass Transf., vol. 25, no. 3 (Apr. 1998) pp. 321-330.
[9]. M. Rudman, H. M. Blackburn, L. J. W Graham, and L. Pullum: Turbulent pipe flow of shear-thinning fluids. J. Nonnewton. Fluid Mech., vol. 118, no. 1. (Mar. 2004) pp. 33-48.
[10]. T. Ohta and M. Miyashita: DNS and LES with an extended Smagorinsky model for wall turbulence in non-Newtonian viscous fluids. J. Nonnewton. Fluid Mech., vol. 206. (Apr. 2014) pp. 29-39.
[11]. M.Rudman, and H. M. Blackburn: Direct numerical simulation of turbulent non-Newtonian flow using a spectral element method. Appl. Math. model. vol. 30, no. 11 (Nov. 2006) pp. 1229-1248.
[12]. P. S. Gnambode, P. Orlandi, M. Ould-Rouiss, and X. Nicolas: Large-Eddy simulation of turbulent pipe flow of power-law fluids. Int. J. Heat Fluid Flow. vol. 54 Aug. 2015 pp. 196-210.
[13]. A. A. Gavrilov and V. Y. Rudyak: Direct numerical simulation of the turbulent flows of power-law fluids in a circular pipe. Thermophys. Aeromechanics, vol. 23, no. 4 (Jul. 2016) pp. 473-486.
[14]. A. A. Gavrilov and V. Y. Rudyak: Direct numerical simulation of the turbulent energy balance and the shear stresses in power-law fluid flows in pipes. Fluid Dyn., vol. 52, no. 3 (May 2017) pp. 363-374.
[15]. Singh, J. Rudman, M. and Blackburn, H. M.: The effect of yield stress on pipe flow turbulence for generalised newtonian fluids. J. Nonnewton. Fluid Mech., vol. 249, (Nov. 2017) pp. 53-62.
[16]. J. Singh, M. Rudman, and H. M. Blackburn: The effect of yield stress on pipe flow turbulence for generalised newtonian fluids. J. Nonnewton. Fluid Mech., vol. 249, (Nov. 2017) pp. 53-62.
[17] M. Abdi, A. Noureddine, and M. Ould-Rouiss, “Numerical simulation of turbulent forced convection of a power law fluid flow in an axially rotating pipe,” J. Brazilian Soc. Mech. Sci. Eng., vol. 42, no. 1, p. 17, 2020.